RSC Advances

ROYAL SOCIETY OF CHEMISTRY

PAPER

View Article Online
View Journal | View Issue

Cite this: *RSC Adv.*, 2026, **16**, 24157

High-performance activated rice straw biochar: a sustainable triple-bottom-line adsorbent for removal of water pharmaceutical pollution

Shimaa Rashad, *[abc] Ahmed A. Farghali, [d] Marwa Waseem A. Halmy, [ab] Hala Elkady, [e] Nadia Badr, [ab] Ahmed Hassan[f] and Heba A. Younes *[g]

Remediation of pharmaceuticals in aquatic systems is crucial due to their substantial environmental and health impacts. In this study, a novel adsorbent from agricultural waste, activated rice straw residue biochar (activated RSR-BC), is developed to overcome the limits of existing water treatment technologies in eliminating sulfamethoxazole (SMX) and clindamycin (CLN) pollutants. Characterization of the synthesized activated RSR-BC adsorbent was done by XRD, SEM, BET, and FTIR to assess its physical and chemical properties. The BET-specific surface area increased after activation by 2.37 times, from 278.92 $m^2\ g^{-1}$ to 662.51 $m^2\ g^{-1}$, and the total pore volume increased. The Activated rice straw residue biochar (activated RSR-BC) showed excellent performance in removing (SMX) and (CLN). The adsorbent demonstrated a theoretical maximum adsorption capacity of 297.4 mg g^{-1} at pH 3 and 184.7 mg g^{-1} at pH 5 for SMX and CLN, respectively. Additionally, a prototype fixed-bed column system demonstrated high efficiency, removing 97.92% of SMX from continuous-flow wastewater effluent within 40 minutes. Beyond targeting specific contaminants, the activated RSR biochar also improved overall wastewater quality by significantly reducing total suspended solids (TSS), chemical oxygen demand (COD), biological oxygen demand (BOD), and total organic carbon (TOC). The main adsorption mechanisms identified include pore-filling, electrostatic attraction, hydrogen bonding, and π–π electron donor–acceptor (EDA) interactions, with chemisorption acting as the rate-limiting step. Moreover, activated RSR-BC material can be reused up to four times with 69.7% removal, highlighting its effectiveness in removing pharmaceuticals from water. Overall, this study demonstrates how agricultural waste, such as rice straw, can be valorized into a high-performance adsorbent for advanced water purification, supporting sustainable development goals (SDGs) and circular economy principles.

Received 3rd February 2026
Accepted 27th April 2026

DOI: 10.1039/d6ra00965d

rsc.li/rsc-advances

1. Introduction

Water scarcity and pollution are among the most pressing global challenges. Only about 3% of Earth's water is freshwater, and less than 1% is accessible as surface water.[1,2] Human activities such as rapid industrialization and urbanization have further degraded limited water resources.[3] Municipal, agricultural, and industrial discharges continuously introduce pollutants into water bodies.[4]

Emerging contaminants (ECs), including pharmaceuticals, personal care products, and industrial chemicals, are of growing concern because they can persist at trace levels, bioaccumulate, enter the food chain, and ultimately threaten human health. Among these, antibiotics such as sulfamethoxazole (SMX), a sulfonamide, and clindamycin (CLN), a lincosamide used mainly against anaerobic infections, are widely prescribed worldwide. These compounds are continuously released into aquatic environments *via* urban wastewater treatment plants (WWTPs), where environmental monitoring has shown that SMX and CLN were detected in concentrations ranging from ng L^{-1} to high μg L^{-1} in waters impacted by wastewater discharges. Typical river waters contain SMX around 60–140 ng L^{-1}, while wastewater streams show 98–2200 ng L^{-1} in WWTP influent and may reach about 35 000 ng L^{-1} in highly

[a]*Natural Resources Sustainability for Land Development Program, Faculty of Science, Alexandria University, Alexandria 21511, Egypt*

[b]*Department of Environmental Sciences, Faculty of Science, Alexandria University, Alexandria 21511, Egypt. E-mail: marwa.w.halmy@alexu.edu.eg; nadia.badr@alexu.edu.eg; Shimaa.Rashad_PG@alexu.edu.eg*

[c]*Basic Sciences Department, Al-Madina Higher Institute for Engineering and Technology, Egypt*

[d]*Materials Science and Nanotechnology Department, Faculty of Postgraduate Studies for Advanced Sciences, Beni-Suef University, Egypt. E-mail: Farghali@psas.bsu.edu.eg*

[e]*Civil Engineering Department, Engineering Research Institute and New and Renewable Energy, National Research Centre of Egypt, NRC, Egypt. E-mail: hala.elkady@gmail.com*

[f]*Department of Civil Engineering, Beni-Suef University, Egypt. E-mail: Ahmedhb96@eng.bsu.edu.eg*

[g]*Environmental Science and Industrial Development Department, Faculty of Postgraduate Studies for Advanced Sciences, Beni-Suef University, Egypt. E-mail: h.ahmed@psas.bsu.edu.eg*

contaminated hospital or influent samples; CLN concentrations in hospital wastewaters range from 184 to 1465 ng L^{-1}, and municipal influent and effluent contain roughly 14–57 ng L^{-1} and up to 151 ng L^{-1}, respectively.[5]

SMX has been reported to exhibit an average removal of about 44%, reflecting its low biodegradability and chemical stability in aqueous matrices. For CLN, several studies have even observed higher concentrations in final effluents than in influents. A detailed mass-flow assessment at a municipal activated-sludge WWTP found that the apparent elimination of CLN ranged from −225% to 3%, indicating that it behaves largely as a conservative, poorly degradable compound; negative "removal" values were attributed to deconjugation of metabolites and additional internal sources rather than true degradation.[6] This phenomenon highlights a complex interaction between clindamycin, sewage components, and hydraulic conditions within the wastewater system.[7] Antibiotics released to the environment at "environmentally relevant" concentrations typically in the ng L^{-1} to low-μg L^{-1} range can still drive antimicrobial resistance (AMR) by selectively enriching resistant bacteria and resistance genes in exposed communities. Reviews of environmental AMR show that WWTPs, receiving rivers, and manure-amended soils frequently contain antibiotic levels that meet or exceed predicted no-effect concentrations for resistance selection, thereby creating hotspots where resistance genes accumulate and are exchanged between environmental, human, and animal microbiota. Even though these concentrations are often below the clinical minimum inhibitory concentrations, laboratory and field studies demonstrate that long-term exposure to sub-inhibitory levels promotes the maintenance and horizontal transfer of resistance determinants, raising serious concern that environmental residues of SMX and CLN contribute to the emergence and global spread of AMR.[8]

Various water treatment methods have been used for emerging contaminants (ECs), including microbial degradation, electrochemical processes, adsorption, membrane filtration, and chemical oxidation. However, these methods have disadvantages, including high operational costs, the generation of secondary pollutants, high energy requirements, and slow kinetics. Adsorption is a cost-effective and efficient method, with a wide range of contaminants.[9] Common adsorbents used for EC removal include activated carbon, silica gel, alumina, polyacrylamide, resins, zeolite, and engineered nanomaterials.[10] Using agricultural residues to produce adsorbents for water purification aligns with the circular economy's principles of waste minimization and resource recovery. Biochar, a porous, carbon-rich material produced by thermochemical conversion of biomass under limited-oxygen conditions, represents a promising solution.[4,11–13] It contributes to various Sustainable Development Goals, notably SDG 6 (Clean Water) and SDG 13 (Climate Action), by enabling pollutant removal while sequestering carbon and utilizing waste biomass.[13] Furthermore, it has a porous structure, a large surface area, abundant functional groups, low cost, and environmental sustainability. Its performance can be tailored by modifying its surface properties. It offers a balance of efficiency and environmental friendliness for water purification.[13,14] Common biochar feedstocks include crop residues, forestry by-products, animal manure, and municipal organic wastes. In wastewater treatment, biochar can adsorb various pollutants, the high surface area and tailored functional groups contribute to its effectiveness, allowing it appropriate for a variety of environmental applications.[1,11,14,15]

While pyrolysis is the most common method for producing biochar, typically carried out at 300–900 °C in an oxygen-limited environment,[11] pristine biochar's adsorption capacity and selectivity can be limited. To overcome this, various physical and chemical modification techniques enhance its properties.[16]

Agricultural waste, particularly rice straw, poses a significant environmental challenge worldwide. Egypt produces approximately 7.86 million tons of rice straw per year, which is commonly disposed of through open burning in fields, a practice that pollutes the environment and is now subject to legislation to limit it.[17] Valorizing this abundant, low-cost agricultural waste into biochar offers a sustainable, cost-effective alternative to expensive, energy-intensive commercial activated carbon for pollutant removal from wastewater.[18]

Biochar primarily removes pollutants through several mechanisms, including adsorption, pore filling, ion exchange, electrostatic attraction, complexation, hydrophobic interactions, hydrogen bonding, and π–π electron donor–acceptor interactions.[14] Beyond direct adsorption, biochar can also function as a filtration medium or a catalyst support for degrading persistent contaminants.[11] Biochar's affordability, simplicity of production, and compatibility with circular economy goals make it a practical option for wastewater treatment.[3,4,18] Modified biochar often achieves removal efficiencies comparable to or exceeding commercial activated carbon at a fraction of the cost.[4,19] However, more pilot-scale studies using real effluents and long-term evaluations are needed to confirm large-scale viability.[4,14]

This study aims to develop and evaluate an innovative, sustainable adsorbent derived from rice straw biochar for the efficient removal of two persistent pharmaceutical pollutants, sulfamethoxazole (SMX) and clindamycin (CLN), from water. Specifically, the objectives are to:[1] Produce rice straw biochar through pyrolysis and enhance it using potassium hydroxide (KOH) activation and ball milling.[2] Characterize the modified biochar to assess improvements in its physicochemical properties relevant to adsorption.[3] Determine the adsorption capacity of the biochar for SMX and CLN through batch experiments and evaluate its practical scalability by operating a prototype fixed-bed column system with real wastewater effluent.

By addressing these objectives, the study demonstrates the potential to transform agricultural waste into a cost-effective, high-performance adsorbent, thereby contributing to sustainable water treatment solutions for emerging pharmaceutical contaminants.

2. Materials and methods

2.1. Preparation of rice straw residue biochar

Rice straw residue (RSR) was collected from a local farm in Beni Suef, Egypt. Sulfamethoxazole (SMX), clindamycin (CLN),

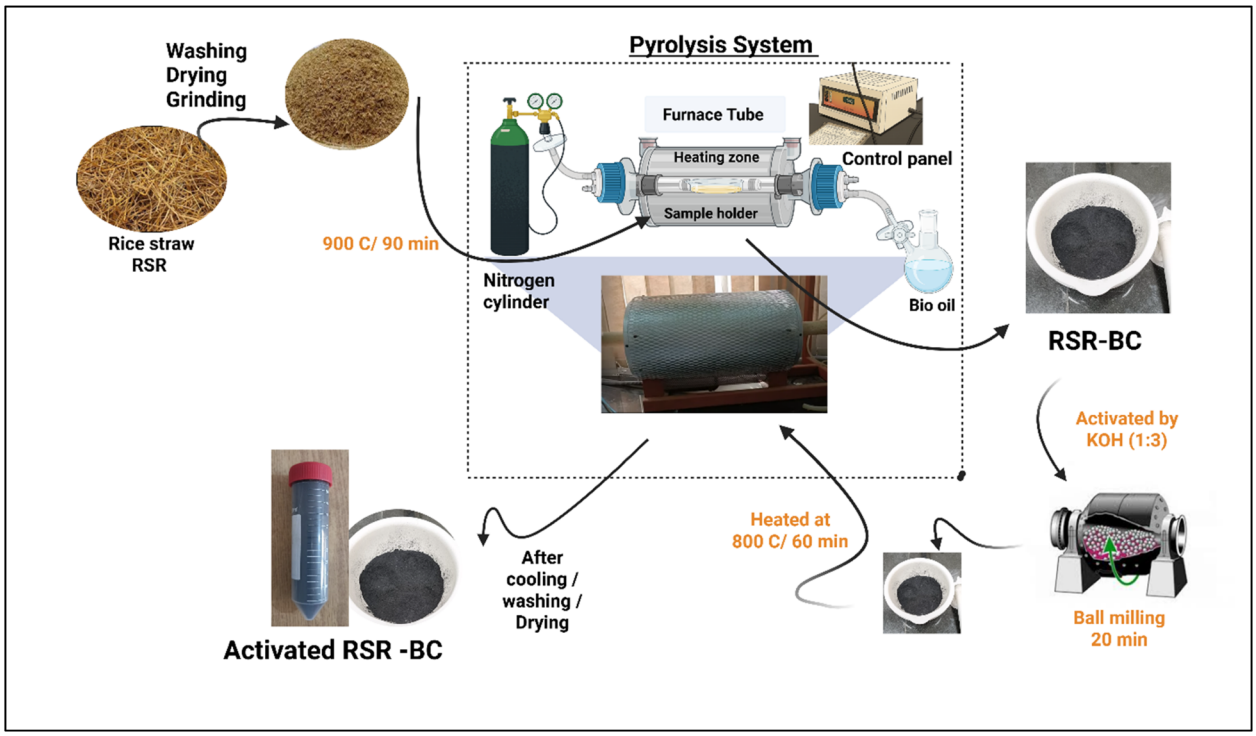

Fig. 1 Schematic diagram of the experimental setup and preparation of activated RSR-BC.

potassium hydroxide (KOH), sodium hydroxide (NaOH), and hydrochloric acid (37%HCl). All the compounds were used as received without additional purification. As shown in the Fig. 1. The Rice straw residue (RSR) sample was washed with distilled water and placed in an oven at 70 °C overnight to remove moisture. The dried rice straw was ground and pyrolyzed in an inert atmosphere at 900 °C in a tube furnace for 90 min to obtain Rice straw biochar (RSR-BC). Nitrogen was selected as the inert gas, and the heating rate was set at 10 °C min^{-1}. After the tube furnace cooled to room temperature, the rice straw was removed and activated with KOH at a 1 : 3 (biochar : KOH) weight ratio. Then, the mixture was ball milled for 20 min and heated at 800 °C for 1 h. After cooling, the sample was washed with 0.5M HCl and distilled water until the solution was neutral. The obtained activated rice straw biochar (activated RSR-BC) was dried in an oven for 24 h at 80 °C.

The selection of 900 °C for pyrolysis and potassium hydroxide (KOH) for chemical activation in this study was strategic, as these conditions are crucial for enhancing the biochar's physicochemical characteristics.[20] Among common chemical activators, KOH is widely regarded as the most effective for generating high-surface-area, strongly microporous carbons, due to its strong etching action and ability to tailor pore structure and surface chemistry, and therefore was selected in this study [21]

2.2. Biochar characterization

Fourier transform infrared (FTIR) analysis of raw material and the resulting biochars was achieved using an ALPHA II (Bruker) with a spectral range from 500 to 4000 cm^{-1}. X-ray diffraction (XRD) (Bruker D8 Advance). The pore characteristics were analyzed using a gas adsorption apparatus (ASAP 2460, Micromeritics). The Brunauer–Emmett–Teller (BET) equation was used to calculate surface area. The surface morphology of biochar was analyzed using scanning electron microscopy (SEM) (JEOL JCM-6000Plus). The pH_{pzc} was measured by the pH drift method.[22]

2.3. Batch adsorption experiments

2.3.1. Batch adsorption of SMX and CLN. Stock solutions of clindamycin (CLM) and sulfamethoxazole (SMX) were made and diluted to a variety of working concentrations to create calibration curves. At room temperature, the prepared activated biochar's adsorption capacity for these antibiotics was examined. Firstly, the effect of pH on adsorption was studied over the range 3–9, where 50 mL of sulfamethoxazole and clindamycin solutions (30 mg L^{-1}) were shaken with 0.01 g of activated biochar at 200 rpm. The pH was adjusted using (0.1 M) sodium hydroxide and hydrochloric acid. At the optimal pH, isotherm studies were conducted over concentrations ranging from 5 to 100 mg L−1, with 0.01 g of activated biochar added to 50 mL of drug solution. To investigate the effect of adsorbent dosage on the removal of SMX, batch adsorption experiments were conducted by varying the mass of activated biochar from 10 to 40 mg while keeping the solution volume (50 mL), initial contaminant concentration (50 mg L^{-1}), and pH 3, while for CLN, initial contaminant concentration was 20 mg L^{-1}, and pH was 5.

The kinetics of SMX & CLN were investigated after various durations ranging from 5 to more than 180 minutes. The samples were shaken at 200 rpm and centrifuged at 8000 rpm for 3 min.

The residual concentration of SMX and CM were subsequently determined by UV-visible spectrometry (T80UV-vis spectrometer). The UV-vis spectra were recorded from 190 to 500 nm, and the maximum absorbance wavelengths were identified at 266 nm for SMX and 192 nm for CLN. The adsorption capacity of (q_e) and the removal rate (R) were calculated according to eqn (1) and (2) respectively:

$$q_e = (C_0 - C_e)V/m \quad (1)$$

$$R(\%) = [(C_0 - C_e)/C_0] \times 100 \quad (2)$$

where q_e is the adsorption quantity of drug on activated biochar at equilibrium, mg g^{-1}; R is the removal rate of SMX or CLN on activated biochar, %; C_0 is the initial concentration of drug mg L^{-1}; C_e is the remaining concentration of drug at equilibrium in mg L^{-1}; V is the volume of system in mL; m is the mass of adsorbent in g.[23]

Three kinetic models (Pseudo-first order kinetic model, pseudo-second order, and Weber–Morris intraparticle diffusion model) were applied to understand the adsorption mechanism of SMX and CLN onto activated biochar. These kinetic models can be represented as follows in eqn (3), (4) and (5)

Pseudo-first order kinetic model:

$$q_t = q_e[1 - \exp(k_1 t)] \quad (3)$$

Pseudo-second order kinetic

$$t/q_t = t/(k_2 q_e^2) + t/q_e \quad (4)$$

where q_t is the adsorption quantity in mg g^{-1}; k_1 is the pseudo-first-rate constant in min^{-1}; k_2 is the pseudo-second-rate constant in g mg^{-1} min^{-1}. The pseudo-first-order and pseudo-second order kinetic models describe the monolayer and multilayer adsorption, respectively.

The intraparticle diffusion data were evaluated using the Weber–Morris model, expressed as:

$$q_t = k_{id} * t^{(1/2)} + C \quad (5)$$

where q_t is the adsorption capacity at time t, k_{id} is the intraparticle diffusion rate constant, and C is the intercept associated with boundary-layer effects.

The isothermal adsorption data were fitted to the Langmuir and Freundlich isothermal adsorption models. These isotherm models can be represented by eqn (6) and (7) respectively:

Langmuir model:

$$q_e = q_m K_L C_e/1 + K_L C_e \quad (6)$$

Freundlish model

$$\ln q_e = \ln K_F + \ln C_e/n \quad (7)$$

where q_e is the amount adsorbed at equilibrium per gram of adsorbent (mg g^{-1}); q_m is maximum monolayer adsorption capacity (mg g^{-1}); K_L is Langmuir model adsorption capacity constant in L $mg^{-}1$; C_e is the equilibrium concentration of adsorbate in solution (mg L^{-1}); K_F is Freundlich adsorption capacity constant in $mg^{1-n} \cdot g^{-1}$ L^n; $1/n$ is Freundlich adsorption intensity constant. The Langmuir model describes monolayer sorption on a homogenous surface, and the Freundlich model explains a multi-layer adsorption process.

The isotherm was categorized by the separation factor R_L, which was defined in eqn 8 to determine the degree of conformance of the Langmuir isothermal model to the adsorption process.

$$R_L = 1/(1 + K_L C_0) \quad (8)$$

where R_L is the parameter to measure the difficult degree of adsorption process, dimensionless parameter; C_0 is the initial concentration of drug solution in mg L^{-1}; K_L is the Langmuir model adsorption capacity constant in L mg^{-1}.[24]

The thermodynamic behavior of adsorption systems is commonly interpreted through the standard Gibbs free energy change (ΔG°), standard enthalpy change (ΔH°), and standard entropy change (ΔS°). In adsorption studies, ΔG° expresses the spontaneity of the process, where negative values indicate thermodynamically favorable adsorption, whereas positive values indicate nonspontaneous behavior under the tested conditions. The temperature dependence of the adsorption equilibrium constant is usually described by the van't Hoff relation, in which a plot of $\ln K$ *versus* $1/T$ allows the estimation of ΔH° from the slope and ΔS° from the intercept. The standard Gibbs free energy change (ΔG°) was obtained from the classical eqn (9) and (10).[25]

$$\Delta G^\circ = \Delta H^\circ - T\Delta S^\circ \quad (9)$$

$$\Delta G^\circ = -RT \ln K_c \quad (10)$$

where R is the gas constant and K_c is the equilibrium reaction constant can be deduced from eqn (11)

$$K_c = q_e/C_e \quad (11)$$

$$\ln K_c = \Delta S^\circ/R - \Delta H^\circ/RT \quad (12)$$

The equilibrium constant expresses the ability of the adsorbent to retain the solute and the extent of its migration into the solution phase; higher K_c values reflect stronger affinity of the sorbent towards the adsorbate. The temperature dependence of the adsorption equilibrium constant is usually described by the van't Hoff relation eqn (12), using this definition, linear plots of $\ln K_c$ *versus* $1/T$ (van't Hoff plots) were constructed, and the values of ΔH°(kJ mol^{-1}) and ΔS°(J mol^{-1} K^{-1}) were calculated from the slope ($-\Delta H^\circ/R$) and intercept ($\Delta S^\circ/R$), respectively.[26]

2.3.2. Application to real wastewater. Batch adsorption tests were conducted to evaluate the elimination of pharmaceuticals and organic matter from several actual wastewater matrices with activated RSR-BC. For SMX adsorption, 30 mg of activated RSR-BC was added to 50 mL of secondary-treated municipal wastewater spiked with 20 ppm SMX; the pH was adjusted to 3, and adsorption occurred with agitation. For CLN, 30 mg of the adsorbent was mixed with 50 mL of similarly

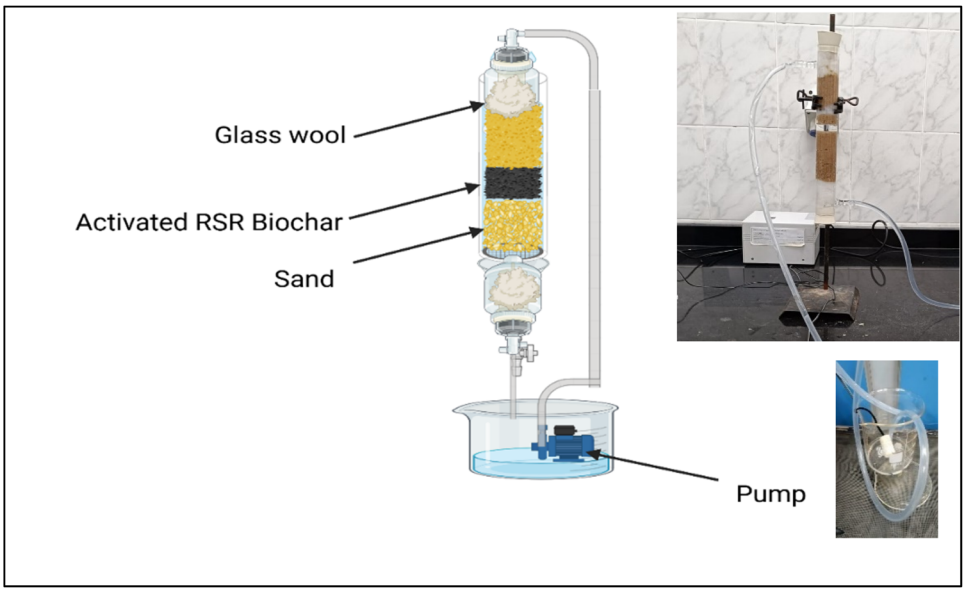

Fig. 2 Scheme of fixed-bed column.

treated effluent, spiked with 20 ppm CLN at pH 5. Different water parameters such as total suspended solids (TSS), chemical oxygen demand (COD), biological oxygen demand (BOD), and total organic carbon (TOC) were examined before and after treatment. Furthermore, 0.5 g of activated RSR-BC was utilized to treat 350 mL of untreated agricultural drainage water, and the same set of water quality parameters was evaluated to determine treatment efficacy.

2.4. Prototype fixed-bed column adsorption

The schematic diagram of the column system is shown in Fig. 2, utilizing fixed beds with continuous flow. It is widely employed in lab-scale adsorption studies because it more realistically simulates actual conditions for sorbent use in adsorption techniques than batch experiments. The fixed bed column system used a glass column (35 cm in height and 5 cm in inner diameter) wet-packed with acid-washed quartz sand above and below the activated biochar layer to stabilize the sorbent and minimize entrapped air. The inlet and outlet of the column were covered with glass wool. After column packing, DI water was pumped through the column to remove bubbles and other impurities. Subsequently, 300 mg of biochar was used. A 200 mL solution of 20 ppm SMX spiked into wastewater effluent was passed through the column. An effluent sample was collected after 40 minutes. Wastewater parameters were also measured before and after adsorption. The aqueous samples were determined using a UV-vis spectrophotometer.

3. Results and discussion

3.1. Characterization of prepared biochar

Scanning electron microscopy (SEM) images, as presented in Fig. 3, clearly reveal the surface morphological changes often documented in the literature, distinguishing the prepared Rice Straw Residue Biochar (RSR-BC) from the activated RSR-BC after activation.[27,28] Fig. 3(a and b) show the pristine RSR-BC exhibited a generally dense structure, limited porosity, and a relatively coarse surface morphology characterized by random cracks. A significant structural modification was observed in the activated RSR-BC Fig. 3(c and d) following activation with potassium hydroxide (KOH) and ball milling. The activated RSR-BC has a more compact and clearly porous structure; the pore architecture was significantly improved by the combination of mechanical ball milling and KOH activation, leading to a higher order and distribution of pores throughout the biochar matrix, this dual treatment not only enhanced the total surface area but also helped to create interconnected pore networks. The dramatic structural transformation observed in the activated RSR-BC is a direct result of the proposed activation mechanism:

Ball milling is a crucial step in the biochar activation process, increasing its surface area and introducing structural defects and microcracks. These defects serve as nucleation sites for pore formation during chemical activation. Ball milling ensures a homogeneous distribution and intimate contact between the KOH activating agent and the carbon matrix, resulting in a more uniform and well-developed porous structure in the final product.

As the temperature rises during the activation process, the KOH begins to crystallize. Simultaneously, the ball-milled, KOH-impregnated biochar undergoes thermal polymerization and curing. This synchronized process leads to the formation of a porous structure, with KOH crystals becoming intricately embedded and stabilized within the pores of the biochar.

As temperature rises, crystalline KOH melts and reacts with biochar carbon, forming potassium-based compounds like K_2CO_3, K_2O, and K metallic potassium. These compounds etch the carbon structure, transforming mesopores and macropores into micropore networks, thereby increasing the material's

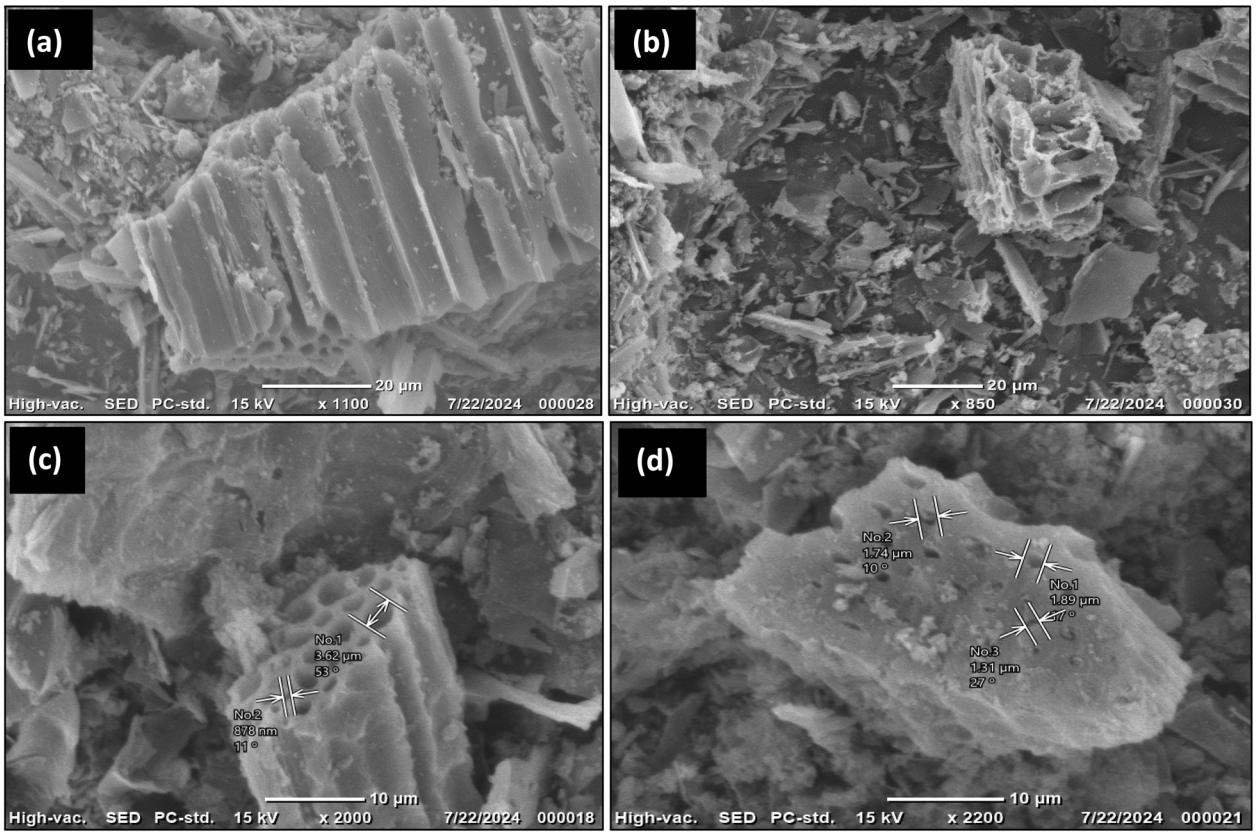

Fig. 3 The SEM morphologies (a and b) rice straw biochar (RSR-BC), and (c and d) activated RSR-BC biochar.

surface area. The main chemical reactions involved in this process are:

$$6KOH + 2C \rightarrow 2K + 3H_2 + 2K_2CO_3$$

$$K_2CO_3 + 2C \rightarrow 2K + 3CO$$

$$K_2O + C \rightarrow 2K + CO$$

$$K_2CO_3 \rightarrow K_2O + CO_2$$

$$2K_2CO_3 \rightarrow 2K_2O + 2CO_2$$

During this stage, gaseous byproducts such as carbon monoxide (CO), carbon dioxide (CO_2), and hydrogen (H_2) are generated and diffused through the pore network, the escape of these gases enhancing micropore formation and resulting in a highly porous biochar with a large specific surface area.

Consequently, after KOH activation and ball milling, SEM images reveal a change in the biochar's surface covered in a network of pores and cavities. KOH activation increases the total pore volume and boosts the amount of micropores and mesopores within the carbon matrix, leading to a larger specific surface area. These profound morphological changes are anticipated to significantly improve the material's adsorption capabilities, particularly for removing of emerging contaminants, such as pharmaceutical drugs from wastewater.[29–32]

For raw rice straw (RSR), the XRD pattern Fig. 4(a) is characterized by several sharp peaks superimposed on a lower, broad background. These sharp peaks are primarily attributed to the crystalline phases present in the raw biomass, most notably crystalline cellulose and silica (SiO_2, quartz). The peaks around $2\theta \approx 22°$, and 34° correspond to the 101, 002, and 040 planes of cellulose, respectively, while a prominent peak near $2\theta \approx 26.6°$ is indicative of silica. The broad background arises from the amorphous components such as lignin and hemicellulose, but the crystalline phases dominate the pattern, reflecting the ordered structure of the raw material.

Upon pyrolysis, the XRD pattern Fig. 4(b) of RSR-BC changes significantly. The sharp peaks associated with cellulose largely disappear, indicating the breakdown of the crystalline cellulose structure during carbonization. The pattern becomes dominated by a broad peak centred around $2\theta \approx 22°$, which corresponds to the 002 plane of disordered, (amorphous) carbon. This broadness reflects the loss of long-range order and the formation of a largely amorphous carbon matrix. Minor peaks from residual minerals, such as silica, may persist, but their intensity is reduced compared to the raw straw.

KOH activation further modifies the XRD pattern in Fig. 4(c) for activated RSR-BC. The (002) peak near $2\theta \approx 22°$ becomes more pronounced, reflecting the partial development of graphitic domains and increased stacking of aromatic layers, but it remains broad, confirming the material is still largely amorphous. The (100) peak near $2\theta \approx 43°$ may also become

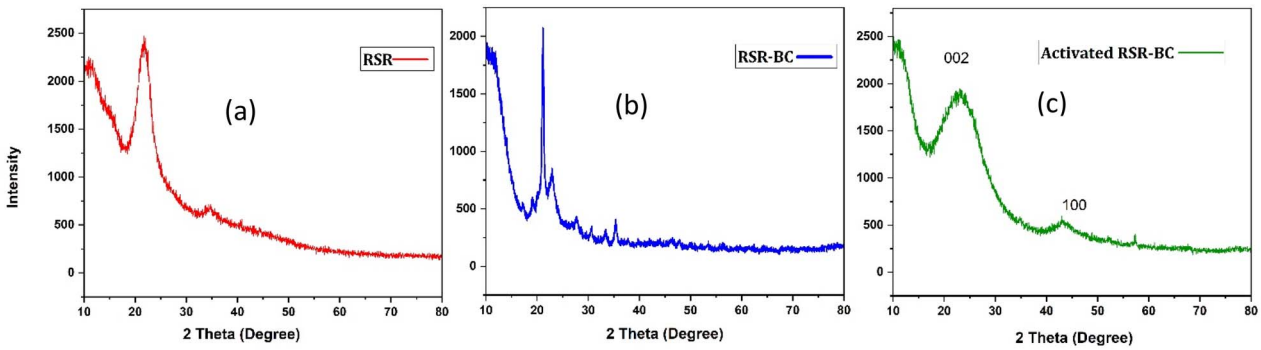

Fig. 4 XRD patterns of (a) rice straw residue, (b) rice straw residue biochar (RSR-BC), and (c) activated rice straw biochar (activated RSR-BC).

more visible, indicating some enhancement in the in-plane ordering of carbon atoms. The overall pattern lacks sharp, well-defined peaks, which is characteristic of amorphous or poorly crystalline carbon materials. The disappearance or reduction of mineral peaks, such as those from silica, suggests that KOH activation removes or transforms some of the inorganic content, further purifying the carbon structure.[29,30,33]

According to the IUPAC classification, the N_2 adsorption–desorption isotherms for RSR-BC and activated RSR-BC Fig. 5(a) show characteristics of both Type I and Type IV isotherms. Type I isotherms reveal that a material has a lot of micropores since they display a steep uptake at low relative pressures because the micropores fill up. Type IV isotherms, on the other hand, are linked to mesoporous materials and show a clear hysteresis loop at higher relative pressures, which is a sign of capillary condensation in mesopores.

The isotherm for the RSR-BC shows that it takes up a moderate amount of nitrogen. As the relative pressure rises, the amount of nitrogen adsorbed goes from about 2 to 7 mmol g^{-1}. This profile shows that there are both micropores and some mesopores, but the surface area and pore volume are not very large.

The isotherm for the activated RSR-BC moves up a lot after activation. As the relative pressure becomes closer to one, the amount of nitrogen adsorbed increases greatly, from roughly 7 to 16 mmol g^{-1}. The activation process generates a hierarchical pore structure with a substantially higher density of both micropores and mesopores. This greatly increases the material's ability to adsorb. The sharper initial uptake at low relative pressures (Type I behaviour) and a clear hysteresis loop at higher pressures (Type IV behaviour). This indicates that a well-defined micro-mesoporous network has formed. This changes by KOH activation chemically etches the carbon matrix, creates new adsorption sites, and greatly increases both the surface area and the total pore volume.

Fig. 5(b) shows the pore size distribution. For (RSR-BC), the pore size distribution is relatively narrow, with most of the pores being in the micropore region (less than 2 nm). The peak pore volume for RSR-BC is about 0.22 $cm^3\ g^{-1}$ at a pore width of about 2 nm. The general distribution quickly drops off as the pore width gets bigger. This means that micropores are the primary type of pore in the inactivated biochar, and mesopores don't grow very much.

After being activated, the activated RSR-BC has a pore size distribution curve that is substantially wider and higher. The highest pore volume for the activated material goes up quickly to about 0.75 $cm^3\ g^{-1}$ at a pore width slightly below 2 nm. The

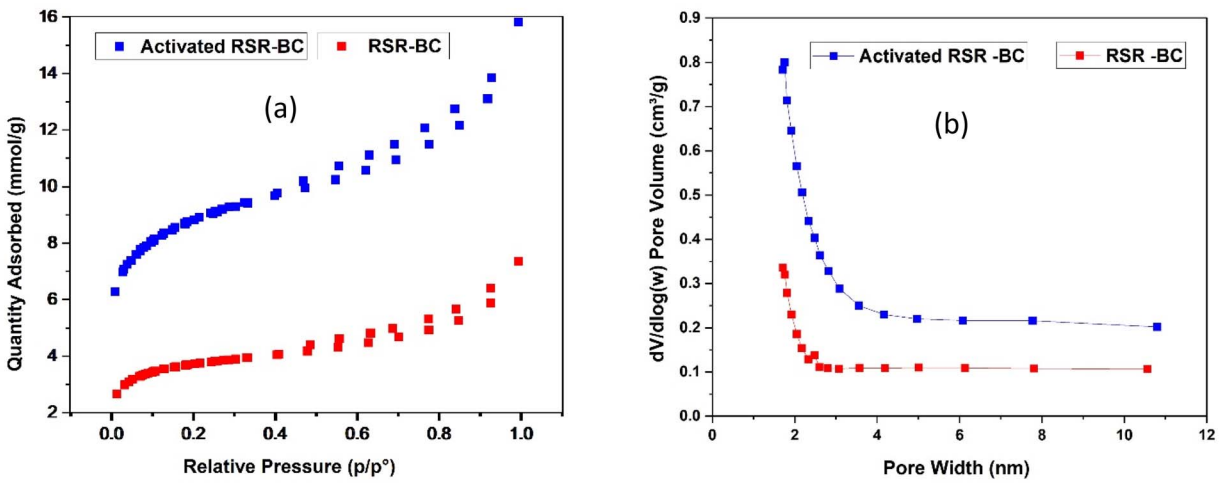

Fig. 5 (a) N_2 adsorption–desorption isotherms of rice straw biochar (RSR-BC) and activated rice straw biochar (activated RSR-BC), (b) pore size distribution of biochar samples.

Table 1 Textural parameters of biochar before and after activation

Parameter	Before activation	After activation
BET surface area ($m^2\ g^{-1}$)	278.9218	662.7257
Micropore area ($m^2\ g^{-1}$)	125.3447	306.6761
External surface area ($m^2\ g^{-1}$)	153.5771	356.0496
Micropore volume ($cm^3\ g^{-1}$)	0.060944	0.148687
Total pore volume ($cm^3\ g^{-1}$)	0.253634	0.543841

distribution also reaches the mesopore region (2–10 nm). The curve's height and width both go up a lot, which shows that activation not only increases the total pore volume but also adds a lot of mesopores to the existing micropores.

As illustrated in Table 1, the modification of the textural parameters of biochar after activation is presented. The BET surface area analysis reveals a significant enhancement in the specific surface area after KOH activation, increasing from 278.9218 $m^2\ g^{-1}$ to 662.5109 $m^2\ g^{-1}$, representing a 2.37-times improvement. This dramatic increase confirms the successful KOH activation process, which creates well-developed pore structures and active functional groups on the biochar surface. The enhanced surface area provides more active sites for adsorption and aligns with the observed improvements in SEM morphology, BJH pore size distribution, and N_2 adsorption–desorption isotherms.

Additionally, the total pore volume increases from 0.25 $cm^3\ g^{-1}$ before activation to 0.54 $cm^3\ g^{-1}$ after activation, while the micropore volume doubles from 0.06 $cm^3\ g^{-1}$ to 0.15 $cm^3\ g^{-1}$. This is consistent with the graphical data, where the area under the curve for the activated sample is much larger, reflecting the creation of a hierarchical pore network with both micropores and mesopores.

The FTIR analysis of rice straw biochar before and after KOH activation as shown in Fig. S1 (see SI) reveals notable changes in the surface chemistry that are crucial for adsorption applications. The spectrum of the RSR-BC displays a broad band around 3445 cm^{-1}, which is attributed to O–H stretching vibrations from hydroxyl groups and adsorbed water. After KOH activation, this band becomes more pronounced, indicating an increased presence of surface hydroxyl groups. The peak at 2922 cm^{-1}, corresponding to aliphatic C–H stretching, remains visible after activation, suggesting that some aliphatic structures are retained. A significant band near 1631 cm^{-1}, associated with C=O stretching (carbonyl/carboxyl) and aromatic C=C bonds, becomes more intense following activation, reflecting increased carbonyl and aromatic functionalities. The peak at 1090 cm^{-1}, assigned to C–O stretching in alcohols, ethers, or esters, is more distinct after activation, indicating the formation of additional oxygen-containing groups. The FTIR peaks observed at 791 cm^{-1}, 629 cm^{-1}, and 467 cm^{-1} in rice straw biochar provide important insights into the material's mineral composition and structural features, particularly after KOH activation. The peak at 791 cm^{-1} is commonly attributed to the presence of quartz, specifically Si–O symmetric stretching or general Si–O vibrations, which are characteristic of biochar derived from silica-rich biomass such as rice straw, the high silica content in rice straw biochar makes the Si–O assignment more prevalent.

The band at 629 cm^{-1} falls within a region typically linked to Si–O bending vibrations or the presence of certain mineral phases, including silicates or phosphates. In the context of rice straw biochar, this peak is most likely due to Si–O–Si bending, indicating the persistence or even enhancement of silicate structures following KOH activation.

Finally, the peak at 467 cm^{-1} is characteristic of Si–O–Si bending vibrations, confirming the presence of silicate minerals within the biochar. The persistence or increased intensity of this peak after KOH activation suggests that the activation process does not remove these mineral phases; rather, it may increase their exposure on the biochar surface, potentially enhancing the material's adsorption properties by providing additional active sites for interaction with contaminants. These observations are consistent with literature studies.[16,29]

The point of zero charge (PZC) of the activated RSR-BC was determined to understand its surface charge characteristics across various pH values. This is significant in understanding its interaction with pollutants at varying pH levels. As shown in Fig. S2 (see SI), the values indicate that the PZC for (activated RSR-BC) is between pH 5.12 and 5.97 across various pH values.[22,34]

This is because at initial pH 3 and 5, the final pH increased, suggesting the biochar surface gained protons (acting as a base) and thus was positively charged. Conversely, at initial pH 7 and 9, the final pH decreased, indicating the biochar surface lost protons (acting as an acid) and became negatively charged. Therefore, the point where the net surface charge is zero, or where initial pH equals final pH, falls within this range, the surface charge of the activated biochar changes with pH, which in turn influences the adsorption of the target antibiotics. Generally, when the solution pH is below the PZC, the biochar surface tends to be positively charged due to protonation of its surface functional groups. Conversely, when the solution pH is above the PZC, the surface becomes negatively charged due to deprotonation.

3.2 Batch adsorption performance

The batch adsorption behaviour of sulfamethoxazole (SMX) and clindamycin (CLN) on (activated RSR-BC) was investigated, revealing distinct characteristics and adsorption patterns.

3.2.1 Effect of pH. The pH of the solution significantly impacted the adsorption of both SMX and CLN onto the activated RSR-BC. As illustrated in Fig. 6(a), the adsorption capacity (q_e) for SMX exhibited a general decrease as the pH increased from 3 to 9, with the highest adsorption observed at pH 3. Conversely, for CLN, the adsorption capacity increased from pH 3 to 5, reaching a peak at pH 5, and then decreased with further increases in pH up to 9.

These variations suggest that the surface charge of the activated biochar and the ionization state of the antibiotic molecules are influenced by pH, which in turn affects the electrostatic interactions governing adsorption.

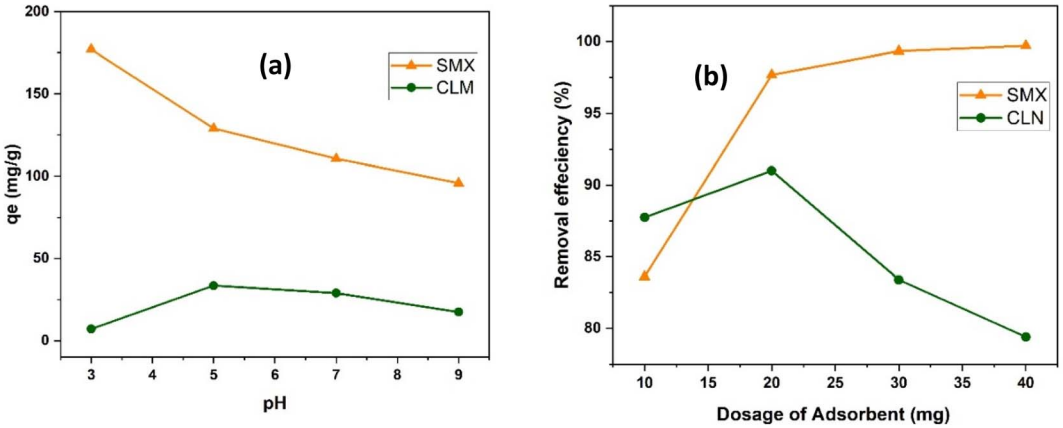

Fig. 6 The effect of (a) pH; (b) adsorbent dosage on the adsorption of both SMX and CLN onto the (activated RSR-BC).

For SMX, the optimal adsorption at acidic pH (pH 3) is attributed to both the neutral/cationic state of SMX below its second pK_a (5.7) and the surface charge of the biochar. At pH 3, near or just below the point of zero charge PZC of RSR biochar (between 5.12 and 5.97), the biochar's surface exhibits a neutral to slightly positive charge, while (SMX) is predominantly neutral. This minimizes electrostatic repulsion, enabling robust π–π interactions and hydrophobic forces to prevail, resulting in significant adsorption. Research indicates that SMX adsorption on biochar is optimal in the acidic to near-neutral range, typically just below or at the point of zero charge (PZC).[35] As the pH increased from 3 to 9, the SMX adsorption capacity consistently decreased. At higher pH values above the PZC of the activated biochar, causing its surface to become negatively charged. Concurrently, SMX becomes increasingly negatively charged at pH > 6. Under these alkaline conditions, electrostatic repulsion occurs between the negatively charged SMX and the negatively charged biochar surface, hindering adsorption.

Concerning CLN, the maximum adsorption at pH 5, which closely aligns with biochar's point of zero charge (5.1–5.9), at this pH, the biochar's surface is shifting from a positive to a negative charge, while clindamycin (pK_a = 7.6) remains positively charged. This state promotes hydrogen bonding and some electrostatic attractions, as the surface is about neutral to slightly negative, while reducing significant repulsive forces that occur at higher pH values when both the surface and adsorbate acquire negative charges.

3.2.2 Effect of adsorbent dosage. Fig. 6(b) illustrates that increasing the adsorbent dosage significantly enhanced the removal efficiency for SMX, with a plateau above 98% at higher dosages. However, CLN removal efficiency initially improved with increased adsorbent dosage reaching a maximum at 20 mg, but it declined with further dosage increases, suggesting factors like particle aggregation or overlapping adsorption sites. This highlights the need for optimizing adsorbent dosage for each target contaminant, as excessive dosages can decrease efficiency. This emphasizes the importance of tailoring adsorbent dosage based on specific physicochemical interactions between the adsorbent and each contaminant.

3.2.3 Effect of contact time and kinetic. The influence of contact time on the adsorption of SMX and CLN over activated RSR-BC. For both antibiotics, the experimental data revealed a rapid initial uptake of the compounds within the first 30 minutes, indicating the availability of readily accessible surface sites on the adsorbent. This rapid phase was followed by a gradual approach to equilibrium. SMX consistently demonstrated a higher adsorption capacity compared to CLN, suggesting a stronger affinity of SMX for the adsorbent surface. The kinetic adsorption behavior exhibited a distinct pattern as illustrated in Fig. 7(a and b). Both the pseudo-first order and pseudo-second-order models provided an excellent fit to the experimental data, demonstrated by high correlation coefficients ($R^2 > 0.99$). Table 2 demonstrates that the pseudo-second-order model yielded a slightly better correlation with the experimental data, with R^2 values of 0.998 for SMX and 0.996 for CLN. Additionally, the calculated q_e values from the pseudo-second-order model (73.3 mg g^{-1} for SMX and 32.6 mg g^{-1} for CLN) closely matched the experimental values. This strong agreement with the pseudo-second-order model suggests that chemisorption might be the rate-limiting step in the adsorption process.

The intraparticle diffusion analysis was fitted using the Weber–Morris model, as illustrated in Fig. 7(e and f), and the corresponding kinetic parameters are summarized in Table 2. The intraparticle diffusion analysis showed that SMX had higher diffusion-related parameters than CLN, with k_{id} of 0.30 ± 0.05 mg g^{-1} $min^{-0.5}$ and C of 69.82 ± 0.49 mg g^{-1}, compared with 0.17 ± 0.05 mg g^{-1} min 0.5 and 30.35 ± 0.51 mg g^{-1} for CLN. The higher C value for SMX suggests a stronger boundary-layer effect and an important role for external mass transfer or surface adsorption in the early stage, while the higher k_{id} indicates a faster intraparticle diffusion contribution. However, the relatively low R^2 values, especially for CLN (0.55), indicate that intraparticle diffusion was not the only rate-controlling step in the adsorption process. Overall, the results point to a multistep adsorption process, beginning with film diffusion and followed by slower diffusion into the adsorbent pores.[36]

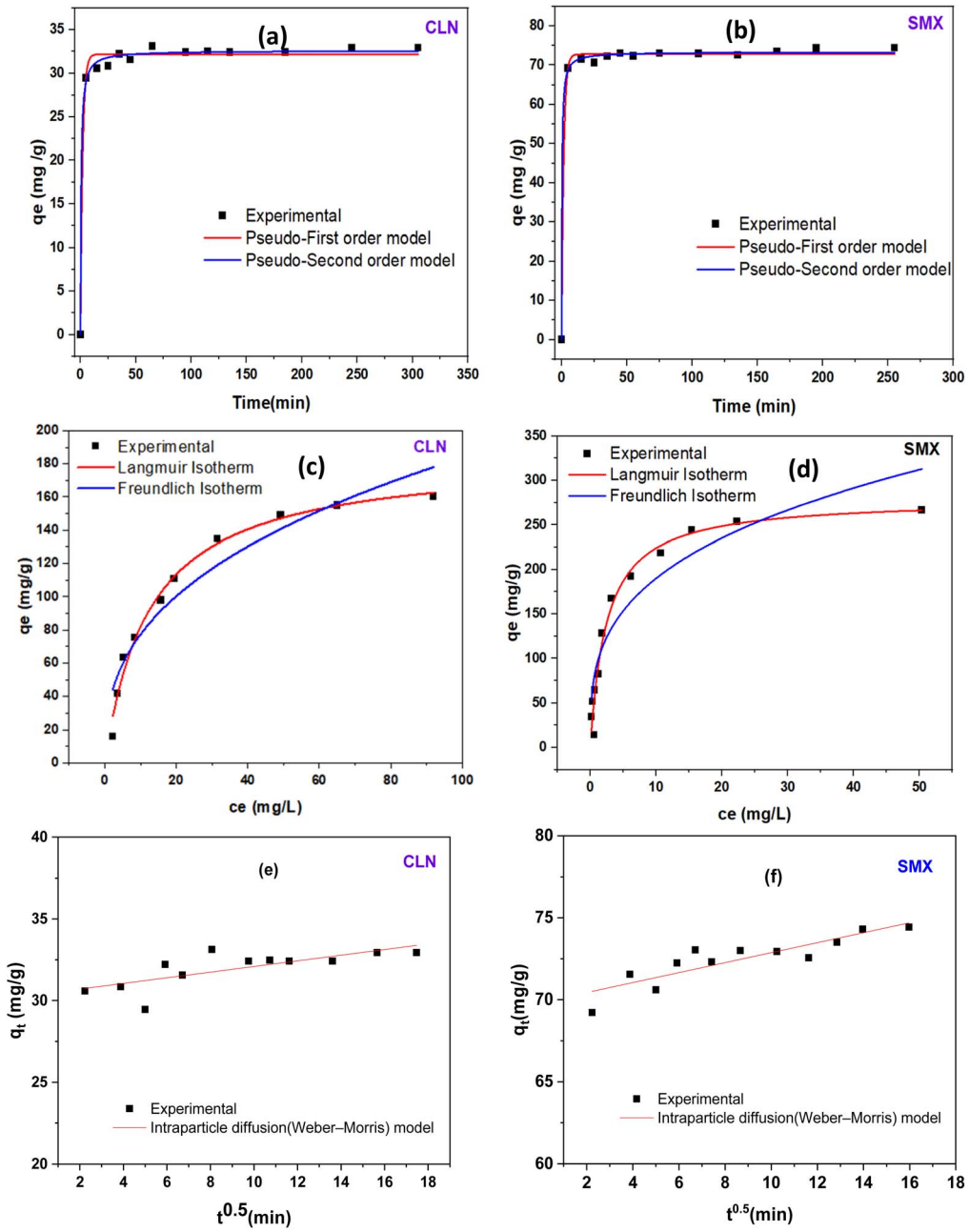

Fig. 7 Kinetic and equilibrium modeling for SMX and CLN adsorption onto activated RSR biochar: (a and b) pseudo-first-order and pseudo-second-order kinetic fits; (c and d) Langmuir and Freundlich isotherm plots; and (e and f) intraparticle diffusion (Weber–Morris) plots.

3.2.4 Adsorption isotherm. The influence of the initial antibiotic concentration on the adsorption process was evaluated, and the experimental data for both SMX and CLN indicated a considerable increase in absorptivity with rising initial concentrations. To further understand the adsorption mechanism, the experimental data were fitted to the Langmuir and Freundlich isotherm models as demonstrated in Fig. 7(c and d). It is characterized by a steep initial uptake at low concentrations, followed by a plateau formation at higher equilibrium concentrations, signifying surface saturation of the adsorbent. As shown in Table 3 the maximum adsorption capacities (q_e) were determined to be 297.4 mg g^{-1} for SMX and 184.7 mg g^{-1} for CLN. The Langmuir isotherm model showed an excellent correlation with the experimental data, yielding high correlation coefficients (R^2) of 0.97 for SMX and 0.98 for CLN. The higher K_L value for SMX (0.4 L mg^{-1}) compared to CLN (0.08 L mg^{-1}) suggests stronger adsorbate–adsorbent interactions for SMX. The Langmuir model describes a monolayer sorption process on a homogenous surface.

The Freundlich isotherm model parameters ($n > 1$ for both compounds) indicated favourable adsorption conditions. The higher n value for SMX (3.2) compared to CLN (2.7) suggests a more heterogeneous surface interaction for SMX. While the

Table 2 Kinetic adsorption model parameters for SMX and CLN on activated RSR biochar

Model	Parameter	CLN	SMX
Experimental	Q_e^{exp} (mg g^{-1})	32.9	74.3
Pseudo-first-order	Q_e (mg g^{-1})	32.2	72.8
	k_1 (min^{-1})	0.5	0.6
	R^2	0.992	0.997
Pseudo-second-order	Q_e (mg g^{-1})	32.6	73.3
	k_2 (g mg^{-1} min^{-1})	0.05	0.04
	R^2	0.996	0.998
Intraparticle diffusion	C (mg g^{-1})	30.35 ± 0.51	69.82 ± 0.49
	k_{id} (mg g^{-1} min$^{-1/2}$)	0.17 ± 0.05	0.30 ± 0.05
	R^2	0.55	0.77

Table 3 Isothermal models parameters for SMX and CLN adsorption by activated RSR-BC

	Langmuir parameters			Freundlich parameters		
Samples	Q_m (mg g^{-1})	K_L	R^2	n	K_F	R^2
Sulfamethoxazole	297.4	0.4	0.97	3.2	93.4	0.88
Clindamycin	184.7	0.08	0.98	2.7	32.5	0.92

Langmuir model provided a slightly better fit in terms of R^2 for CLN, the Freundlich R^2 values were 0.88 for SMX and 0.92 for CLN, indicating good fits and suggesting a multi-layer adsorption process as explained by the Freundlich model.

The adsorption capacities summarized in Table 4 and 5 show that activated RSR-BC outperforms many reported materials for SMX and CLN removal, with q_{max} values exceeding those of most carbonaceous and biochar-based adsorbents cited in the literature. This comparison highlights the strong affinity of RSR-BC for both target antibiotics and confirms its potential as a competitive adsorbent for advanced wastewater treatment applications.

3.2.5 The effect of temperature on thermodynamic parameters. The influence of temperature on the adsorption performance of SMX and CLN by the prepared activated biochar is illustrated in Fig. 8(a), whereas the corresponding Van't Hoff plots ($\ln K_c$ *versus* $1/T$) are shown in Fig. 8(b). Thermodynamic parameters derived from these plots are summarized in Table 6, For SMX, the Van't Hoff line exhibited a high correlation coefficient ($R^2 = 0.9886$), with $\Delta H^\circ = 139.0$ kJ mol^{-1} and $\Delta S^\circ = 478$ J mol^{-1} K^{-1}. The calculated ΔG° values were −5.95, −11.55, and −15.49 kJ mol^{-1} at 303, 313, and 323 K, respectively, indicating that SMX adsorption is spontaneous at all investigated temperatures and becomes more thermodynamically favorable as temperature increases, in line with other reports of endothermic, entropy-driven SMX uptake on carbonaceous adsorbents. The relatively large positive ΔH° confirms the endothermic nature of the process and suggests that additional energy is required to overcome solvation and activate surface sites, while the positive ΔS° reflects increased randomness at the solid–solution interface, which may be associated with desorption of structured water and rearrangement of SMX at the biochar surface.[46]

In contrast, CLN exhibited a weaker temperature response, corresponding to $\Delta H^\circ = 83.1$ kJ mol^{-1} and $\Delta S^\circ = 262$ J mol^{-1} K^{-1}. The calculated ΔG° values for CLN were 4.51, −0.31 and −0.62 kJ mol^{-1} at 303, 313 and 323 K, respectively, indicating that adsorption is not spontaneous at 303 K but becomes only slightly favorable at higher temperatures. Overall, the thermodynamic parameters confirm that increasing temperature enhances adsorption of both pharmaceuticals, but the effect is much more pronounced for SMX, for which the process is strongly endothermic, entropy-driven, and spontaneous over the whole temperature range studied.

3.2.6 Adsorption mechanism. The adsorption of pharmaceutical compounds onto activated biochar's surface is a complex process influenced the material's physicochemical properties and the characteristics of the adsorbate molecules. Several mechanisms collectively govern the removal of sulfamethoxazole (SMX) and clindamycin (CLN) by this activated biochar Fig. 9. Firstly, the pore-filling mechanism is

Table 4 Adsorption capacities of various adsorbents for SMX removal from aqueous solutions

Adsorbent	q_{max} (mg g^{-1})	Ref.
Activated RSR-BC	297.4	Current study
Ordered mesoporous carbon	334	37
Graphene nanoplatelets	210.1	38
Graphene-like carbon from lignin	289.2	39
Graphene nanosheets	103	40
Graphene oxide sheets	122	40
Magnetic chitosan beads	≈200	41
H_3PO_4-modified sludge-based biochar	45.6	35
Amine-functionalized activated carbon	≈53.5	42
Biomass-derived activated carbon	≈160.5	43

Table 5 Adsorption capacities of various adsorbents for CLN/lincomycin removal from aqueous solutions

Adsorbent	q_{max} (mg g^{-1})	Ref.
Activated RSR-BC	184.7	Current study
Ag_2S-chitosan nanocomposite	153.2	44
Ag_2S-chitosan nanohybrid	181.3	44
H_3PO_4-modified sludge-based biochar	26.6	35
Graphene oxide nanosheets	47	45

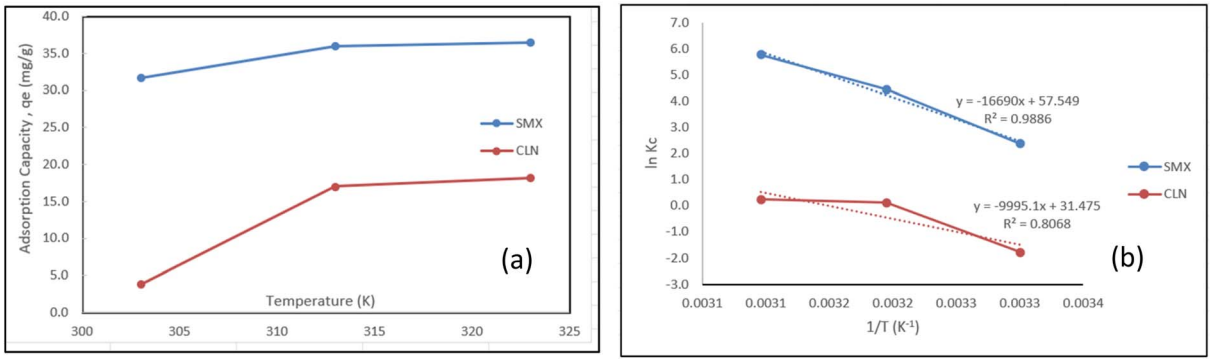

Fig. 8 (a) The effect of temperature on adsorption of SMX and CLN on activated RSR-BC, (b) Van't Hoff plot.

Table 6 Parameters of thermodynamics for the adsorption of SMX & CLN on activated RSR-BC

Adsorbate	Van't Hoff equation	R^2	ΔH° (kJ mol^{-1})	ΔS° (J mol^{-1} K^{-1})	ΔG° (kJ mol^{-1})		
					303 K	313 K	323 K
SMX	$y = -16690x + 57.549$	0.9886	139.0	478	−5.95	−11.55	−15.49
CLN	$y = -9995.1x + 31.475$	0.8068	83.1	262	4.51	−0.31	−0.62

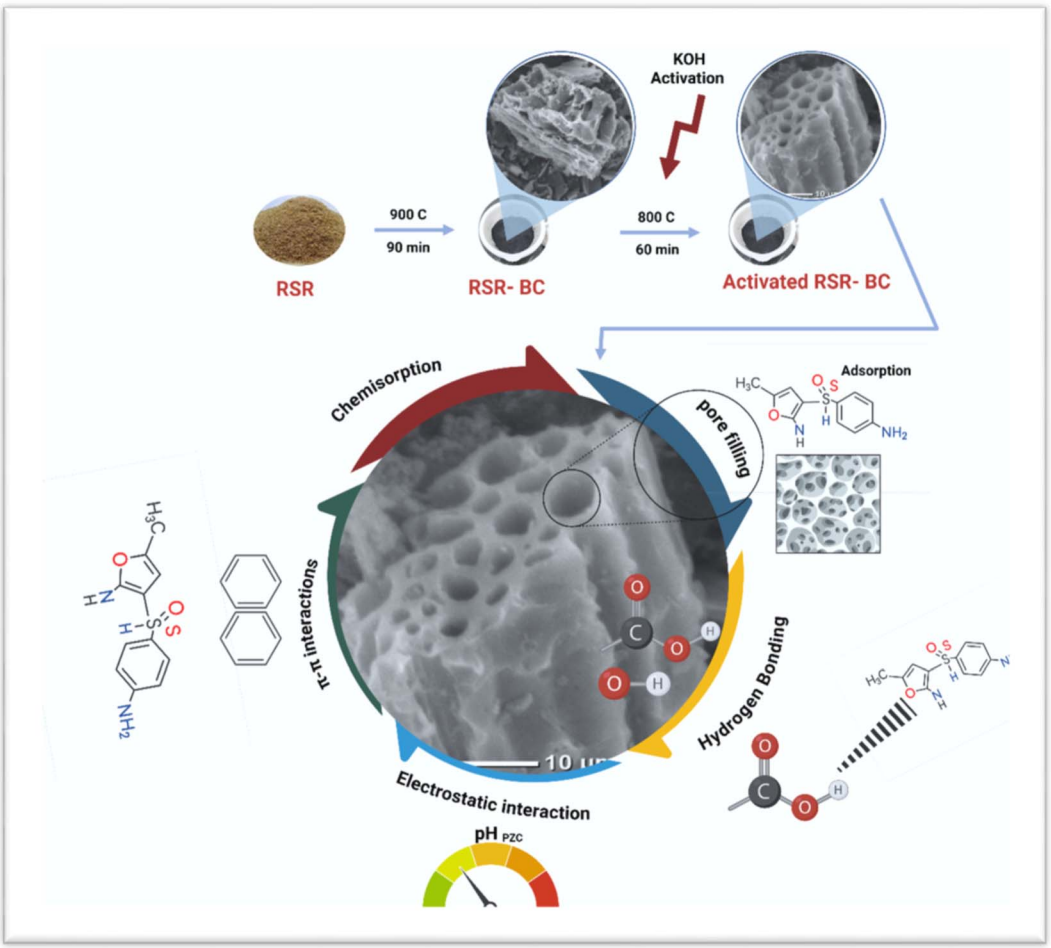

Fig. 9 The adsorption mechanism of SMX &CLN on the activated RSR-BC.

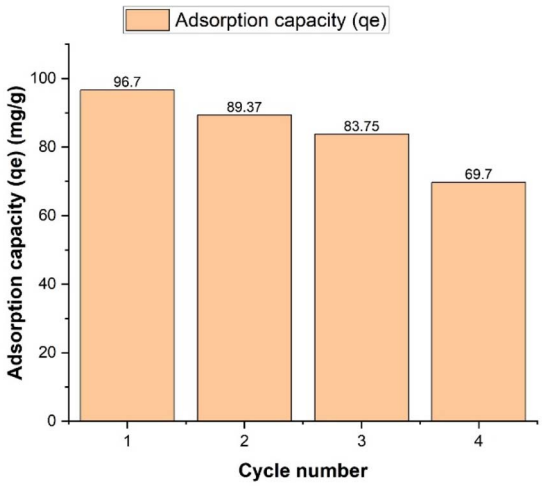

Fig. 10 The effect of reusability of activated RSR BC for SMX.

crucial due to the biochar's significantly enhanced specific surface area, increasing from 278.9218 m^2 g^{-1} to 662.5109 m^2 g^{-1}. This is coupled with an increase in total pore volume from 0.253634 cm^3 g^{-1} to 0.543841 cm^3 g^{-1} and visually confirmed by scanning electron microscopy (SEM) images showing a well-developed porous structure with micro- and mesopores. This extensive pore network, including micron-sized pores, allows for the efficient entrapment of adsorbate molecules.

Secondly, electrostatic interactions are crucial in the adsorption profiles of SMX and CLN, as shown by the pH-dependent adsorption profiles. The activated RSR biochar has a point of zero charge between pH 5.12 and 5.97, with the biochar surface positively charged below and negatively charged above. The highest adsorption for SMX occurs at pH 3, where the biochar surface is positively charged, facilitating electrostatic attraction with the neutral SMX species. For CLN, adsorption peaks at pH 5, consistent with optimal surface charge and ionization state.[47]

Thirdly, hydrogen bonding is a significant mechanism, supported by Fourier-Transform Infrared (FTIR) analysis which confirms the enhancement of oxygen-containing functional groups on the activated biochar surface after KOH activation. These groups, such as hydroxyl (O–H stretching at 3445 cm^{-1}), carbonyl/carboxyl (C=O stretching near 1631 cm^{-1}), and C–O stretching at 1090 cm^{-1}, serve as crucial sites for forming hydrogen bonds with polar moieties present in SMX and CLN molecules.[28]

Fourthly, π–π electron donor–acceptor (EDA) interactions are involved. X-ray diffraction (XRD) analysis indicates the development of graphitic structures in the activated RSR biochar, with distinct (002) and (100) peaks appearing at approximately 23° and 43° respectively. This, combined with the increase in aromatic C=C bonds noted in FTIR spectra after activation, provides a rich aromatic surface. SMX, an aromatic sulfonamide, exhibits superior adsorption due to molecular-level interactions with the aromatic domains of biochar. It forms strong π–π electron donor–acceptor interactions, hydrogen bonding, and pore filling. The structure of SMX, consisting of aromatic and heterocyclic rings, enables high-affinity, multi-mechanism adsorption. Its small size allows efficient access to biochar's microporous structure.[33] The activated biochar, with its graphitic regions and oxygen-containing functional groups (C=C, OH, C=O), serves as an effective electron donor, facilitating these interactions with SMX, which can act as a π-electron acceptor due to its aromatic rings and electron-withdrawing groups. In contrast, clindamycin (CLN) lacks aromatic rings, so π–π interactions cannot occur, limiting adsorption to mechanisms such as hydrogen bonding and electrostatic attraction. In addition, CLN's larger structure restricts penetration into fine pores, resulting in a lower total adsorption capacity than SMX on the surface of biochar.[35]

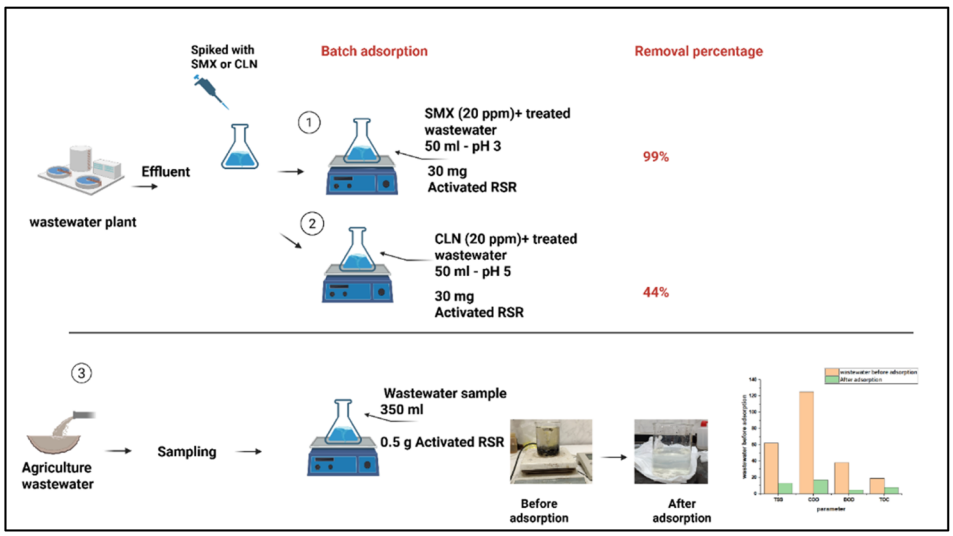

Fig. 11 Batch adsorption with real wastewater experiment.

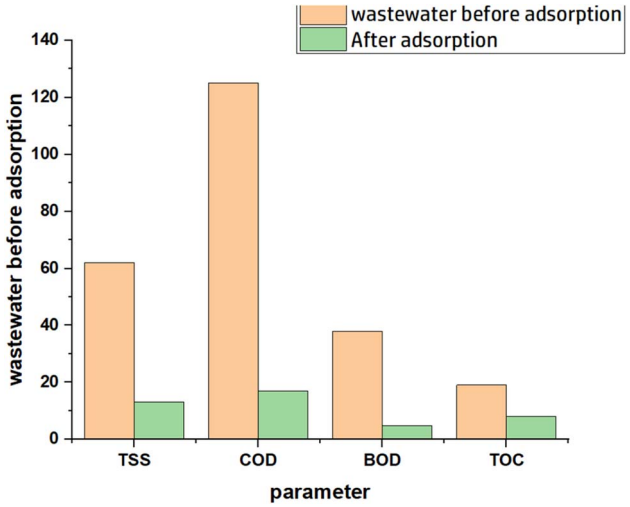

Fig. 12 Water quality parameter before and after adsorption by using activated RSR BC.

Finally, the chemisorption-dominated mechanism is highlighted by kinetic studies for both SMX and CLN, where the pseudo-second-order (PSO) model provides a superior fit to the experimental data with high correlation coefficients (R^2 values of 0.998 for SMX and 0.996 for CLN). This strong agreement suggests that chemisorption, involving chemical reactions like electron sharing or transfer between the pharmaceuticals and the biochar's functional groups, is the rate-limiting step in the adsorption process. This includes interactions like hydrogen bonding and π–π EDA. While the Langmuir isotherm also fits well, indicating monolayer adsorption, the overall data fitting implies that both physical and chemical interactions are involved in the adsorption process.[47]

3.2.7 The regeneration & reusability evaluation. The reusability and regeneration of adsorbents are critical for ensuring the economic efficiency and sustainability of wastewater treatment processes. This study aimed to demonstrate this key aspect by converting agricultural waste, specifically rice residue into an effective adsorbent for the removal of antibiotics, addressing a significant global problem of persistent water pollution. The valorization of biomass into high-value adsorbents like biochar represents a viable waste management solution and offers raw materials at a reduced cost, making it a promising and sustainable approach.

The prepared (activated RSR-BC) exhibited promising regeneration performance, Fig. 10 indicating its potential for sustainable use. The ability of biochar to be reactivated and reused for multiple cycles significantly reduces operational and running costs compared to single-use adsorbents the gradual reduction in adsorption capacity observed over successive cycles is a commonly expected and well-documented trend in reusability and regeneration studies of adsorbents. This decline, as seen in your Sulfamethoxazole (SMX) data where capacities decreased from 96.7 mg g^{-1} in Cycle 1 to 69.7 mg g^{-1} in Cycle 4. This is primarily attributed to several key factors. These may include incomplete desorption of the pollutant, which leaves residual adsorbate occupying active sites.

3.2.8 Application to real wastewater batch adsorption. The activated rice straw residue (RSR) biochar's efficacy in removing pollutants was rigorously demonstrated through several batch adsorption experiments utilizing different water matrices (Fig. 11).

In experiment 1, focused on SMX removal from wastewater effluent, the activated RSR biochar proved highly effective, with a nearly complete removal of approximately 99.27% was achieved within a short 15-minute adsorption period. This rapid, highly efficient removal process highlights biochar's strong affinity for SMX under these batch conditions. Experiment 2 addressed Clindamycin (CLN) removal from wastewater effluent. After 3 hours of adsorption, an approximate 44.44% reduction in the initial CLN concentration was observed. Beyond the specific removal of clindamycin, this adsorption process also significantly improved several general wastewater quality parameters. Total Suspended Solids (TSS) were reduced by approximately 70.83%, Chemical Oxygen Demand (COD) decreased by approximately 85.00%, Biochemical Oxygen Demand (BOD) was reduced by at least 75.00%, and Total

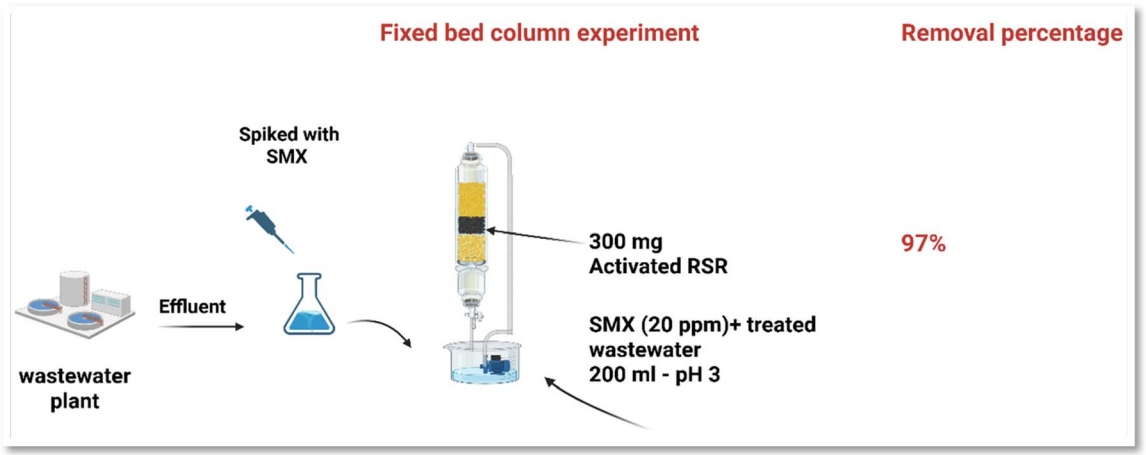

Fig. 13 Fixed bed column adsorption experiment.

Organic Carbon (TOC) saw a reduction of at least 72.22%. These comprehensive improvements highlight the broad efficacy of activated RSR-BC in improving overall wastewater quality. Finally, Experiment 3 involved the batch treatment of real agricultural drainage wastewater for 1 hour. This process led to substantial reductions in key parameters as shown in Fig. 12. TSS decreased by approximately 79.03%, COD by approximately 86.40%, BOD by approximately 86.84%, and TOC by approximately 57.89%.

3.2.9 Fixed bed column adsorption. Fig. 13 illustrates the experimental setup for the fixed-bed column adsorption. In this Experiment concerning SMX removal in a continuous flow fixed bed column, the system was initiated with SMX spiked in wastewater effluent. After 40 minutes of flow through the column, approximately 97.92% of the SMX was removed from the continuous flow system within the tested duration. The fixed bed column setup by using activated RSR-BC also demonstrated considerable improvements in general wastewater parameters. TSS was reduced approximately 22.22%. COD saw a significant decrease, indicating a reduction of approximately 72.16%. BOD, corresponding to a reduction of approximately 85.71%. TOC showing a reduction of approximately 66.67%. These findings confirm the robust performance of (activated RSR-BC) in a continuous flow system, effectively removing target antibiotics and enhancing overall wastewater quality.

4. Conclusion

This study demonstrated that the activated rice straw residue biochar (activated RSR-BC) is an effective and sustainable adsorbent for removing pharmaceutical emerging contaminants, specifically sulfamethoxazole (SMX) and clindamycin (CLN), from wastewater. The critical activation with potassium hydroxide (KOH) combined with ball milling significantly enhanced the biochar's physicochemical properties, increasing its specific surface area and total pore volume. Morphological analysis confirmed the formation of a well-developed porous structure with an extensive network of micro- and mesopores. Chemical characterization further revealed a higher abundance of surface functional groups and the development of graphitic structures, providing more active sites for adsorption.

Both batch experiments and a prototype fixed-bed column system demonstrated the activated RSR-BC's excellent removal efficiency for SMX and CLN in real wastewater. Beyond these targeted pharmaceuticals, the biochar also improved overall wastewater quality by substantially reducing total suspended solids (TSS), chemical oxygen demand (COD), biochemical oxygen demand (BOD), and total organic carbon (TOC). The material's promising reusability and regeneration performance highlight its cost-effectiveness and environmental benefits. Overall, this study validates the valorization of agricultural waste, specifically rice straw, into a high-performance, sustainable adsorbent for advanced water treatment, directly supporting multiple Sustainable Development Goals (SDGs) and the principles of the circular economy.

Author contributions

Shimaa Rashad: conceptualization, data curation, formal analysis, methodology, writing – original draft, review & editing. Ahmed A. Farghali: validation, resources, methodology Marwa Waseem A. Halmy: writing – review & editing, data curation, supervision Hala Elkady: writing – review & editing, supervision, methodology, investigation conceptualization Nadia Badr: validation, conceptualization, supervision Ahmed Hassan: validation, investigation, conceptualization Heba A. Younes: writing – review & editing, investigation, methodology, data curation.

Conflicts of interest

The authors declare no conflict of interest regarding the publication of this article.

Data availability

The datasets generated and/or analyzed during the current study are available from the corresponding author upon reasonable request.

Supplementary information (SI) is available. See DOI: https://doi.org/10.1039/d6ra00965d.

References

1 F. Obar, M. Alherbawi, G. Mckay and T. Al-Ansari, Optimizing the utilization of biochar from waste: an energy–water–food nexus assessment approach considering water treatment and soil application scenarios, *Front. Environ. Sci.*, 2023, **11**, 1238810, DOI: 10.3389/fenvs.2023.1238810.

2 P. Viotti, S. Marzeddu, A. Antonucci, M. A. Décima, P. Lovascio, F. Tatti, *et al.*, Biochar as Alternative Material for Heavy Metal Adsorption from Groundwaters: Lab-Scale (Column) Experiment Review, *Materials*, 2024, **17**(4), 809, DOI: 10.3390/ma17040809.

3 R. Li, Y. Wu, X. Lou, H. Li, J. Cheng, B. Shen, *et al.*, Porous Biochar Materials for Sustainable Water Treatment: Synthesis, Modification, and Application, *Water*, 2023, **15**(3), 395, DOI: 10.3390/w15030395.

4 B. Díaz, A. Sommer-Márquez, P. E. Ordoñez, E. Bastardo-González, M. Ricaurte and C. Navas-Cárdenas, Synthesis Methods, Properties, and Modifications of Biochar-Based Materials for Wastewater Treatment: A Review, *Resources*, 2024, **13**(1), 8, DOI: 10.3390/resources13010008.

5 M. Ekwanzala, R. Lehutso, T. Kasonga, J. Dewar and M. Momba, Environmental Dissemination of Selected Antibiotics from Hospital Wastewater to the Aquatic Environment, *Antibiotics*, 2020, **9**(7), 431, DOI: 10.3390/antibiotics9070431.

6 C. Marx, N. Günther, S. Schubert, R. Oertel, M. Ahnert, P. Krebs, *et al.*, Mass flow of antibiotics in a wastewater treatment plant focusing on removal variations due to

operational parameters, *Sci. Total Environ.*, 2015, **538**, 779–788, DOI: 10.1016/j.scitotenv.2015.08.112.

7 R. Oertel, S. Schubert, V. Mühlbauer, B. Büttner, C. Marx and W. Kirch, Determination of clindamycin and its metabolite clindamycin sulfoxide in diverse sewage samples, *Environ. Sci. Pollut. Res.*, 2014, **21**(20), 11764–11769, DOI: 10.1007/s11356-013-2333-2.

8 D. G. J. Larsson and C. F. Flach, Antibiotic resistance in the environment, *Nat. Rev. Microbiol.*, 2022, **20**(5), 257–269, DOI: 10.1038/s41579-021-00649-x.

9 S. Kathi and M. A. El Din, Trends in effective removal of emerging contaminants from wastewater: A comprehensive review, *Desalination Water Treat.*, 2024, **317**, 100258, DOI: 10.1016/j.dwt.2024.100258.

10 N. Cheng, B. Wang, P. Wu, X. Lee, Y. Xing, M. Chen, *et al.*, Adsorption of emerging contaminants from water and wastewater by modified biochar: A review, *Environ. Pollut.*, 2021, **273**, 116448, DOI: 10.1016/j.envpol.2021.116448.

11 S. K. Cho, B. Igliński and G. Kumar, Biomass based biochar production approaches and its applications in wastewater treatment, machine learning and microbial sensors, *Bioresour. Technol.*, 2024, **391**, 129904, DOI: 10.1016/j.biortech.2023.129904.

12 G. S. Ghodake, S. K. Shinde, A. A. Kadam, R. G. Saratale, G. D. Saratale, M. Kumar, *et al.*, Review on biomass feedstocks, pyrolysis mechanism and physicochemical properties of biochar: State-of-the-art framework to speed up vision of circular bioeconomy, *J. Clean. Prod.*, 2021, **297**, 126645, DOI: 10.1016/j.jclepro.2021.126645.

13 M. He, Z. Xu, D. Hou, B. Gao, X. Cao, Y. S. Ok, *et al.*, Waste-derived biochar for water pollution control and sustainable development, *Nat. Rev. Earth Environ.*, 2022, **3**(7), 444–460, DOI: 10.1038/s43017-022-00306-8.

14 G. Enaime, A. Baçaoui, A. Yaacoubi and M. Lübken, Biochar for Wastewater Treatment—Conversion Technologies and Applications, *Appl. Sci.*, 2020, **10**(10), 3492, DOI: 10.3390/app10103492.

15 L. Leng, Q. Xiong, L. Yang, H. Li, Y. Zhou, W. Zhang, *et al.*, An overview on engineering the surface area and porosity of biochar, *Sci. Total Environ.*, 2021, **763**, 144204, DOI: 10.1016/j.scitotenv.2020.144204.

16 W. T. Tsai, Y. Q. Lin and H. J. Huang, Valorization of Rice Husk for the Production of Porous Biochar Materials, *Fermentation*, 2021, **7**(2), 70, DOI: 10.3390/fermentation7020070.

17 E. Abdel Hamid, M. Ismail, M. Moussa, M. Abdel Aziz, M. Sobhy, R. Mohamed, Y. Mohamed, *et al.*, Optimization and Characterization of Bio-Silica Extraction from Rice Straw Using RSM, *Egypt. J. Chem.*, 2023, **66**(11), 373–383, DOI: 10.21608/ejchem.2023.161205.6968.

18 T. M. Tichem, Y. Wang, R. B. H. Gameli, B. Mbage and B. Li, Multicomponent Adsorption of Pollutants from Wastewater Using Low-Cost Eco-Friendly Iron-Modified Rice Husk Biochar in the Era of Green Chemistry, *Sustainability*, 2023, **15**(23), 16348, DOI: 10.3390/su152316348.

19 F. Amalina, S. Krishnan, A. W. Zularisam and M. Nasrullah, Pristine and modified biochar applications as multifunctional component towards sustainable future: Recent advances and new insights, *Sci. Total Environ.*, 2024, **914**, 169608, DOI: 10.1016/j.scitotenv.2023.169608.

20 M. E. Wahyu, D. Damayanti and H. S. Wu, Production, Characterization, and Application of KOH-Activated Biochar from Rice Straw for Azo Dye Adsorption, *Biomass*, 2025, **5**(3), 40, DOI: 10.3390/biomass5030040.

21 C. Quan, N. Miskolczi, S. Feng, P. Grammelis, C. Wu and N. Gao, Effect of type of activating agent on properties of activated carbon prepared from digested solid waste, *J. Environ. Manage.*, 2023, **348**, 119234, DOI: 10.1016/j.jenvman.2023.119234.

22 M. M. Bin, N. S. Pinky, S. Mustafi, F. Chowdhury, A. Nahar, U. S. Akhtar, *et al.*, Unveiling the reactor effect: a comprehensive characterization of biochar derived from rubber seed shell *via* pyrolysis and in-house reactor, *RSC Adv.*, 2024, **14**(41), 29848–29859, DOI: 10.1039/D4RA05562D.

23 Z. Yi, J. Yao, M. Zhu, H. Chen, F. Wang and X. Liu, Kinetics, equilibrium, and thermodynamics investigation on the adsorption of lead(II) by coal-based activated carbon, *SpringerPlus*, 2016, **5**(1), 1160, DOI: 10.1186/s40064-016-2839-4.

24 N. A. A. Salim, M. H. Puteh, M. H. Khamidun, M. A. Fulazzaky, N. H. Abdullah, A. R. M. Yusoff and M. Nuid, Interpretation of isotherm models for adsorption of ammonium onto granular activated carbon, *Biointerface Res. Appl. Chem.*, 2021, **11**(2), 9227–9241, DOI: 10.33263/BRIAC112.92279241.

25 G. Amin, S. Konstantinovic, I. Jordanov and D. Djordjevic, THERMODYNAMICS OF TEXTILE CATIONIC DYE ADSORPTION ON CLINOPTILOLITE, *Stud. Univ. Babes-Bolyai, Chem.*, 2023, **27**, 179–192, DOI: 10.24193/subbchem.2023.1.13.

26 E. C. Lima, A. Hosseini-Bandegharaei, J. C. Moreno-Piraján and I. Anastopoulos, A critical review of the estimation of the thermodynamic parameters on adsorption equilibria. Wrong use of equilibrium constant in the Van't Hoof equation for calculation of thermodynamic parameters of adsorption, *J. Mol. Liq.*, 2019, **273**, 425–434, DOI: 10.1016/j.molliq.2018.10.048.

27 J. Cheng, Y. Lu, Y. Sun, S. Deng, H. Yang, M. Zhang, *et al.*, Impact of Activation Conditions on the Electrochemical Performance of Rice Straw Biochar for Supercapacitor Electrodes, *Molecules*, 2025, **30**(3), 632, DOI: 10.3390/molecules30030632.

28 Y. Sun, L. Zheng, X. Zheng, D. Xiao, Y. Yang, Z. Zhang, *et al.*, Adsorption of Sulfonamides in Aqueous Solution on Reusable Coconut-Shell Biochar Modified by Alkaline Activation and Magnetization, *Front. Chem.*, 2022, **21**, 9, DOI: 10.3389/fchem.2021.814647.

29 S. Bashir, J. Zhu, Q. Fu and H. Hu, Comparing the adsorption mechanism of Cd by rice straw pristine and KOH-modified biochar, *Environ. Sci. Pollut. Res.*, 2018, **25**(12), 11875–11883, DOI: 10.1007/s11356-018-1292-z.

30 R. Nandi, M. K. Jha, S. K. Guchhait, D. Sutradhar and S. Yadav, Impact of KOH Activation on Rice Husk Derived Porous Activated Carbon for Carbon Capture at Flue Gas

alike Temperatures with High CO_2/N_2 Selectivity, *ACS Omega*, 2023, **8**(5), 4802–4812, DOI: 10.1021/acsomega.2c06955.

31 J. Qu, Y. Wang, X. Tian, Z. Jiang, F. Deng, Y. Tao, *et al.*, KOH-activated porous biochar with high specific surface area for adsorptive removal of chromium (VI) and naphthalene from water: Affecting factors, mechanisms and reusability exploration, *J. Hazard. Mater.*, 2021, **401**, 123292, DOI: 10.1016/j.jhazmat.2020.123292.

32 M. J. Saad, C. H. Chia, S. Zakaria, M. S. Sajab, S. Misran, M. H. Abdul Rahman, *et al.*, Physical and Chemical Properties of the Rice Straw Activated Carbon Produced from Carbonization and KOH Activation Processes, *Sains Malays.*, 2019, **48**(2), 385–391, DOI: 10.17576/jsm-2019-4802-16.

33 E. Avramiotis, Z. Frontistis, I. D. Manariotis, J. Vakros and D. Mantzavinos, Oxidation of Sulfamethoxazole by Rice Husk Biochar-Activated Persulfate, *Catalysts*, 2021, **11**(7), 850, DOI: 10.3390/catal11070850.

34 E. Avramiotis, Z. Frontistis, I. D. Manariotis, J. Vakros and D. Mantzavinos, On the Performance of a Sustainable Rice Husk Biochar for the Activation of Persulfate and the Degradation of Antibiotics, *Catalysts*, 2021, **11**(11), 1303, DOI: 10.3390/catal11111303.

35 S. Minaei, K. Zoroufchi Benis, K. N. McPhedran and J. Soltan, Adsorption of sulfamethoxazole and lincomycin from single and binary aqueous systems using acid-modified biochar from activated sludge biomass, *J. Environ. Manage.*, 2024, **358**, 120742, DOI: 10.1016/j.jenvman.2024.120742.

36 K. H. Chu, M. A. Hashim, M. H. Zawawi and J. C. Bollinger, The Weber–Morris model in water contaminant adsorption: Shattering long-standing misconceptions, *J. Environ. Chem. Eng.*, 2025, **13**(4), 117266, DOI: 10.1016/j.jece.2025.117266.

37 P. Sarker, X. Lei, K. Taylor, W. Holmes, H. Yan, D. Cao, *et al.*, Evaluation of the adsorption of sulfamethoxazole (SMX) within aqueous influents onto customized ordered mesoporous carbon (OMC) adsorbents: Performance and elucidation of key adsorption mechanisms, *Chem. Eng. J.*, 2023, **454**, 140082, DOI: 10.1016/j.cej.2022.140082.

38 F. A. Rosli, H. Ahmad, K. Jumbri, A. H. Abdullah, S. Kamaruzaman and N. A. Fathihah Abdullah, Efficient removal of pharmaceuticals from water using graphene nanoplatelets as adsorbent, *R. Soc. Open Sci.*, 2021, **8**(1), 201076, DOI: 10.1098/rsos.201076.

39 L. P. Lingamdinne, G. K. R. Angaru, B. Shrestha, J. R. Koduru and R. R. Karri, High-performance adsorption of sulfamethoxazole and phenol using graphene-like carbon derived from glucose, *Sci. Rep.*, 2026, **16**(1), 7794, DOI: 10.1038/s41598-026-39165-4.

40 R. Rostamian and H. Behnejad, A comparative adsorption study of sulfamethoxazole onto graphene and graphene oxide nanosheets through equilibrium, kinetic and thermodynamic modeling, *Process Saf. Environ. Prot.*, 2016, **102**, 20–29, DOI: 10.1016/j.psep.2015.12.011.

41 D. Pirozzi, A. Latte, A. Yousuf, F. De Mastro, G. Brunetti, A. El Hassanin, *et al.*, Magnetic Chitosan for the Removal of Sulfamethoxazole from Tertiary Wastewaters, *Nanomaterials*, 2024, **14**(5), 406, DOI: 10.3390/nano14050406.

42 Q. K. Nguyen, T. T. T. Phan, N. B. Tran, D. D. Tran, T. M. Nguyen, B. Pham, *et al.*, Enhanced adsorption of sulfamethoxazole antibiotic on amine grafted activated carbon using (3-Aminopropyl) triethoxysilane (APTES), *Mater. Chem. Phys.*, 2025, **339**, 130782, DOI: 10.1016/j.matchemphys.2025.130782.

43 M. A. Zamiri and C. H. Niu, Investigation of mechanisms of sulfamethoxazole adsorption on novel adsorbents developed from reed canary grass, *Chem. Eng. Commun.*, 2025, **212**(1), 75–93, DOI: 10.1080/00986445.2024.2398253.

44 V. K. Gupta, A. Fakhri, S. Agarwal and M. Azad, Synthesis and characterization of Ag 2 S decorated chitosan nanocomposites and chitosan nanofibers for removal of lincosamides antibiotic, *Int. J. Biol. Macromol.*, 2017, **103**, 1–7, DOI: 10.1016/j.ijbiomac.2017.05.018.

45 L. Mohammad nejad, Y. Pashaei, B. Daraei, M. Forouzesh and shekarchi maryam, Graphene oxide-based dispersive-solid phase extraction for preconcentration and determination of ampicillin sodium and clindamycin hydrochloride antibiotics in environmental water samples followed by HPLC-UV detection, *Iran. J. Pharm. Res.*, 2019, **18**(2), 642–657, DOI: 10.22037/ijpr.2019.1100676.

46 I. Ijaz, A. Bukhari, A. Nazir, E. Gilani, H. Zain, A. Shaheen, *et al.*, Simultaneous adsorption of sulfamethoxazole and neodymium from wastewater by a MXene-, α-aminophosphonate-, and sulfated fucan-based ternary composite based on anion-synergistic interactions, *RSC Adv.*, 2025, **15**(7), 5042–5059, DOI: 10.1039/D4RA08766F.

47 M. C. Ndoun, H. A. Elliott, H. E. Preisendanz, C. F. Williams, A. Knopf and J. E. Watson, Adsorption of pharmaceuticals from aqueous solutions using biochar derived from cotton gin waste and guayule bagasse, *Biochar*, 2021, **3**(1), 89–104, DOI: 10.1007/s42773-020-00070-2.